Automation in Construction 89 (2018) 292–298

Contents lists available at ScienceDirect

Automation in Construction

journal homepage: www.elsevier.com/locate/autcon

An algorithm for automatic localization and detection of rebars from GPR data of concrete bridge decks

Kien Dinh[a,*], Nenad Gucunski[b], Trung H. Duong[c]

[a] CONSEN Inc., Montréal, Canada
[b] Department of Civil & Environmental Engineering, Rutgers University, USA
[c] Department of Engineering, Colorado State University-Pueblo, Pueblo, CO, USA

ARTICLE INFO

Keywords:
Ground penetrating radar
Rebar detection
Automation
Image processing
Convolutional neural network
Deep learning
Bridge inspection

ABSTRACT

Picking rebars manually in the data from ground penetrating radar (GPR) surveys of concrete bridge decks is time consuming and labor intensive. This paper presents an automated rebar localization and detection algorithm for performing this task. The proposed methodology is based on the integration of conventional image processing techniques and deep convolutional neural networks (CNN). In the first step, the image processing methods, such as the migration, normalized cross correlation and thresholding, are used to localize pixels containing potential rebar peaks. In the second step, windowed images surrounding the potential pixels are first extracted from the raw GPR scans involved in the first step. Those are then classified by a trained CNN. In the process, likely true rebar peaks are recognized and retained, whereas likely false positive detections are discarded. The implementation of the proposed system in the analysis of GPR data for twenty-six bridge decks has shown excellent performance. In all cases, the accuracy of the proposed system has been greater than 95.75%. The overall accuracy for the entire deck library was found to be 99.60% ± 0.85%.

1. Introduction

The use of ground penetrating radar (GPR) in the condition assessment of concrete bridge decks has been well recognized and accepted. This technology provides data of high resolution and quality that can be employed to evaluate various aspects of the deck condition. Specific applications of GPR include evaluation of the deck thickness, localization of rebars in concrete, or measurement of the concrete cover [1]. Furthermore, it can be applied to characterize concrete deterioration, delamination potential, to describe concrete as a corrosive environment, or to estimate the concrete's dielectric constant and conductivity [1–10]. On the other hand, a large amount of data, which the GPR produces, requires extensive manual processing to extract useful pieces of information. Of all the processes, the identification and localization of rebar peaks from B-scans (rebar picking) is well known to be the most labor intensive and time consuming.

Particularly, the manual efforts will be multiplied with the use of multi-channel GPR systems, such as those described in [11]. In such situations, it may take several working days, or even weeks, for a GPR analyst to complete the rebar-picking task for a single bridge deck. Consequently, GPR might not be a cost-effective option and not be considered for deck condition evaluation. In addition, the manual method of picking rebar prevents real-time data processing in the robotics assisted bridge inspection [11]. Motivated by these issues, the main goal of this study was to develop an algorithm that will automate the localization and detection of rebar peaks from GPR data.

Automatic detection of buried objects, in general, and rebars, in particular, in GPR images has attracted much research interest from researchers in different science disciplines. For instance, Al-Nuaimy et al. [12] developed an automatic system that recognizes solid objects, such as pipes and anti-personnel landmines, in GPR images. In the first step of their algorithm, GPR images are segmented using feature extraction and neural networks (NNs) classification. In the second step, the regions classified as target reflections, i.e., reflections from solid objects, are further processed with edge detection and pattern recognition algorithms to identify precise locations of the objects under investigation.

In another study, Gamba and Lossani [13] utilized NNs to investigate hyperbolic signatures of pipes in GPR images. Specifically, a NN detector was developed and applied to find buried objects on GPR images after the images had undergone some pre-processing steps. The purpose of those steps was to enhance the visibility of the signatures of buried objects. Pasolli et al. [14] developed a technique based on a genetic algorithm (GA) to recognize, in binary images, linear and

* Corresponding author.
E-mail addresses: kien.dinh@consen.ca (K. Dinh), gucunski@soe.rutgers.edu (N. Gucunski), trung.duong@csupueblo.edu (T.H. Duong).

https://doi.org/10.1016/j.autcon.2018.02.017
Received 2 August 2017; Received in revised form 4 February 2018; Accepted 7 February 2018

hyperbolic signatures of solid, subsurface objects. By using the features extracted from those binary objects, a support vector machine (SVM) classifier was used to categorize them into linear or hyperbolic shapes.

Krause et al. [15] proposed a method that utilizes image segmentation in the detection of rebar objects. Specifically, an image segmentation technique was employed to first isolate arcs in the GPR B-scans. An arc detector was then applied to categorize those based on how well they match a hyperbolic shape. An arc with the highest rating would be regarded as a hyperbolic rebar signature. When the technique was tested on simple GPR scans, the accuracy was reported to be approximately 90%. Such accuracy, however, greatly decreased when the same technique was applied to complicated GPR profiles.

Similar to the detection of pipe signatures mentioned above, a NN was used for the detection of rebars in [16]. Specifically, to identify hyperbolic rebar patterns, the study first used an image processing technique for edge detection. The detected edge lines were then divided into a set of overlapping sections that were used to search hyperbolic patterns using the NN. The technique was demonstrated through a correct localization of two reinforcing bars in a concrete slab. It was, however, evident that the layout of rebars in real concrete decks, and accordingly in real GPR images, is much more complicated than the one used as an illustration in that case study.

In a more recent study [17], a template matching and a hyperbolic curve-fitting algorithm were employed to detect reinforcing steel bars. In the first step, a sum of squared difference (SSD) was utilized to evaluate the similarity between a sliding window of GPR images and a hyperbolic rebar template. When the SSD attained a minimum value, a reference rebar position was selected. Then, with an assumption that the spacing between rebars was fixed, a Fast Fourier Transform (FFT) was used to find the hyperbolic peaks of all the remaining rebars. Finally, a hyperbolic curve fitting was executed to find the parameters of each hyperbola using partial differential equations. There are a few limitations of the approach. The first and biggest limitation is that the template image would need to be selected manually for each bridge deck. The second limitation is the assumption of a fixed rebar spacing, which is not true in many cases. Further limitation is stemming from the fact that the SSD is not a good similarity metric for the template matching for these types of problems. The reason is that, an SSD is affected by the absolute intensity values of the pixels of the two images under comparison. GPR data for different decks, on the other hand, may be collected by different gain setups. Similarly, different rebars in the same deck may be at sections with various degrees of deterioration and, therefore, may have very different amplitudes of reflection.

The methodology proposed in [18] is the most recently presented technique. It uses a SVM classifier to categorize regions in a GPR image into two groups: groups containing, and those not containing rebar signatures. The input of such a classifier is the histogram of oriented gradients (HOG), which is extracted from each windowed image region. After finding likely rebar regions from the SVM classifier, the method uses a hyperbola-fitting algorithm to find rebar peaks in GPR profiles. The proposed methodology was demonstrated in GPR surveys of two real concrete decks with a correct rebar detection of 92.45% and 91.50%, respectively.

2. Research methodology

This study proposes the use of deep convolutional neural networks (CNN) for identification of hyperbolic rebar pattern, after conventional image processing techniques have been employed to localize potential rebar peaks. While the entire process for an automatic rebar picking is summarized in Fig. 1, each of the steps will be described in detail in the subsequent sections.

2.1. Time-zero correction

The setting of zero time position is of high importance for determining correct values of the two-way travel time and, consequently, the rebar depth when processing GPR data. For an air-coupled antenna, the zero time corresponds to the reflection from the ground surface. On the other hand, for a ground-coupled antenna, it corresponds to the direct-coupling reflection. Conventionally, the zero time is placed at either the negative or the positive maximum peaks of the first wavelet. As those peaks do not represent the true time-zero position, the current research employs the zero time as suggested in a previous study [19]. Specifically, the zero time is located at 0.61 ns before the positive peak in the first GPR wavelet. Programmatically, that first positive peak can be searched easily for each GPR signal (A-scan) in a B-scan. After the position of the first positive peak was found for all A-scans, an averaging operation is performed to find the average position of the first positive peak for the entire B-scan. The B-scan will then be corrected for time-zero by discarding all the samples before 0.61 ns of the average position of the first positive peak. A section of a B-scan before and after time-zero correction using the proposed procedure is illustrated in Fig. 2.

2.2. Migration

The purpose of migration is to collapse all hyperbolic patterns associated with reinforcing bars, and to find their true locations. This step should only be done after GPR scans have been corrected for time-zero. A comparison between an original GPR scan, collected by a 1.5-GHz ground-coupled antenna, and the one after migration is provided in Fig. 3a and b. The signal velocity used in the migration was 0.1 m/ns.

A number of different methods for performing migration exist [20]. The hyperbolic summation (HS) migration algorithm was selected for this study. This technique is effective and very easy to understand and, therefore, is most commonly used. Specifically, in the HS algorithm, each pixel with a positive amplitude value in the original GPR image is migrated by guessing all possible locations of reflecting objects. Once this was completed, the amplitude values of pixels at a true object location will end up having the sum amplitude value of all the pixels on the hyperbola. Therefore, in the migrated GPR scans, the energy will be focused on true locations of reflecting objects. On the other hand, the amplitude of a pixel that is not at the apex of a hyperbola will become relatively small compared to those of the pixels at the true rebar location.

In addition, it should be noted that when performing a migration it is very important to select a correct signal velocity. If the velocity selected for the migration operation is lower or higher than the true signal velocity, it will result in “under-migration” or “over-migration”, respectively. Examples of under-migration and over-migration are depicted in Fig. 3c and d, where a signal velocity of 0.07 and 0.13 m/ns were used, respectively. Based on those definitions of migration, and our trial and error experiments for GPR surveys on a large number of concrete bridge decks, a signal velocity of 0.1 m/ns has been selected in this research. That led to correctly-migrated B-scans, as depicted in Fig. 3b. Certainly, one may be concerned with the variation of signal velocity within a single concrete deck, or variations between different decks. As it will be shown later, this assumed velocity worked well for all bridge decks in this study.

2.3. Localization of potential rebar peaks

To clarify the automated rebar-picking algorithm, details of two main steps of the algorithm are described. The first step aims at localizing potential rebar peaks, and is performed on migrated profiles. In the second step, the spatial information of the pixels containing potential rebar peaks in the migrated scans are used to determine the locations of potential rebar peaks in the non-migrated scans. As expected, since the migration operation does not change the size and number of pixels in the GPR scans, the spatial information will be the same for both raw and migrated profiles. Finally, small images

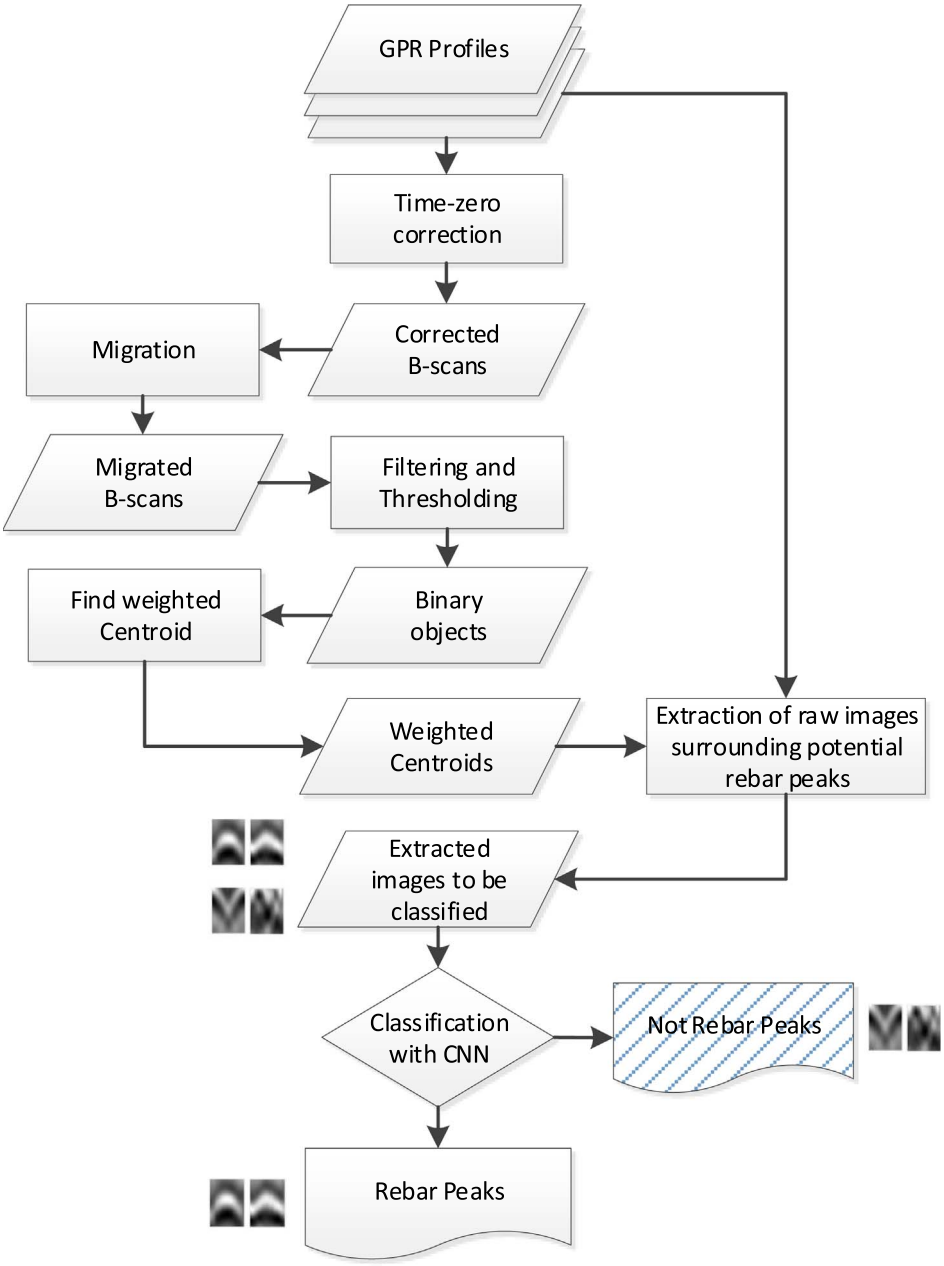

Fig. 1. Automatic rebar picking process.

surrounding potential rebar peaks are extracted from the non-migrated GPR scans to be later classified by a CNN as whether it contains, or not, rebar signatures. Examples of extracted images (51 × 37 pixels) from raw GPR profiles were provided in Fig. 1.

It is obvious that localizing rebar peaks from migrated B-scans is much easier than localizing the same from original GPR images. First, the migrated profiles provide a higher intensity contrast than the original images. Second, the dot rebar signature in a migrated B-scan is more stable, compared to the parameters of hyperbolic shapes in the original images that are subjected to a rebar depth variation. It is the changes of those parameters that have resulted in a limited success of the template matching method in detecting hyperbolic rebar signatures. Therefore, instead of doing the template matching on original GPR images, the matching operation in this study was performed on migrated profiles. After a careful analysis of "dot" rebar signatures on migrated GPR scans, a simple "*match filter*" has been developed, as presented in Fig. 4.

Specifically, the filter is parametrically designed so that its vertical size (in pixels) corresponds to 1.0 ns of the two-way travel time, whereas the horizontal size corresponds to a 0.1 m distance. While the intensity value of all pixels close to the external boundary of the filter is zero, the intensity value of the pixels near the center is unity. Since the area in the center has approximately the same shape and size of the rebar signatures in migrated GPR profiles, it will facilitate the filtering of rebar objects. In terms of the operation, the filter will be slid over all possible regions in the migrated B-scans. For each position, a normalized cross correlation (NCC) coefficient will be computed to compare the similarity between the sub-regions of migrated B-scans with the filter. The closer to unity the NCC coefficient is, the higher the possibility that a rebar exists at that sub-region will be.

It is worth noting that the goal of the selection of filter size was to limit the effects of unwanted reflections from a delamination or neighboring bars on the filtering operation. For example, if the filter is too big, two rebars may be included in the sub-region to be compared

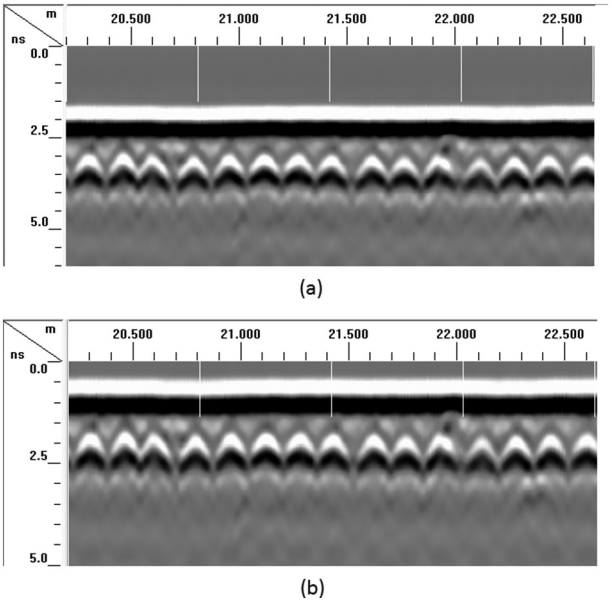

Fig. 2. B-scans: (a) before and (b) after time-zero correction.

with the filter. That will result in a lower NCC coefficient for the sub-region and the automatic rebar picking may miss the two rebars. On the other hand, the filter needs to be large enough to cover migrated rebar signatures. Considering commonly found rebar sizes in concrete bridge decks, for example about 16 mm (bar #5); the size selected for the filter in this study will be appropriate in most cases.

Finally, with respect to the thresholding, a global threshold of 0.45 for the NCC coefficient has been selected based on the evaluation of GPR data for a number of bridge decks. This threshold is small enough to pick up the most of binary objects containing rebar peaks, but is also large enough to separate the binary objects between different bars, and those from unwanted reflections. The rebar peak for each rebar can then be precisely defined within each binary object by finding a weighted centroid of that binary object in the original GPR image. As can be seen in Fig. 5, although being able to pick up all the rebar peaks, the filtering and thresholding step also results in many false positive (FP) rebar detections. For example, there are false detections right below many true rebar locations in Fig. 5. Those are caused by the tails of reflection wavelets at the top rebar level. All these false positive detections are eliminated in the next step.

2.4. Elimination of false rebar peaks using deep learning

There are, in general, two methods for elimination of false positive rebar detections. In the first method, a number of picking criteria is used to discard false detections. For example, using a priori knowledge of a common range of rebar depth, all the binary objects that lie above or below a certain number of pixels can be removed. Other picking criteria can be used, such as common rebar spacing, expected shapes and areas of binary objects that contain rebar peaks, etc. As can be seen in Fig. 5, binary objects that contain rebars have a distinct stable round shape. However, this approach is not preferred, because it may need to be fine-tuned for each particular bridge deck.

In the second method, a classifier is used to recognize, if the image containing a potential peak represents a rebar or not. This classifier can be built based on machine learning techniques, such as SVM or traditional neural networks. These machine learning-based classifiers, however, require a feature vector (region descriptors) input to be extracted from each image section. Its performance, therefore, will depend on how well the selected feature vector describes the objects under investigation. For example, Kaur et al. [18] compared different feature vectors and concluded that the HOG provided the best performance for their SVM classifier.

It was also recognized that a deep learning technique, the so-called deep convolutional neural networks (CNN), could be employed to solve the classification problem in this study. A CNN is a class of deep, feed-forward artificial neural networks (ANNs) with multiple hidden layers. This deep (multiple layers) structure allows a CNN to learn representations of data with multiple levels of abstraction [21]. Therefore, for a classification problem, it works directly with data in their raw form and does not require a feature vector to be manually designed with an exceptional level of expertise.

In the presented algorithm, the locations of potential rebar peaks (pixels) identified from the migrated profiles are first used to extract small image sections surrounding those pixels. Those are done from the original or non-migrated GPR scans. A CNN will then be used to classify those images into two categories: (1) images containing rebars, and (2) images not containing rebars. It is again noted that, because the CNN has an inherent ability to discover automatically the representation needed for detection and classification, there is no need to extract any feature vectors. Therefore, it is expected herein that by simply feeding the CNN with thousands of example images, both positive (containing rebars) and negative (not containing rebars), the CNN will be trained to fulfill its functionality of detecting rebar signatures.

A MATLAB program has been written to implement the above process. A data set of 4000 example GPR images has been extracted from raw GPR profiles for training and testing of the CNN. Of those 4000, 3000 images were used as the training set and 1000 images as the testing set. The number of positive and negative samples in each of these two sets are equal. All the images have the same size of 51×37 pixels and were extracted from B-scans of two bare reinforced concrete bridge decks. The GPR data were collected using a 1.5 GHz ground-coupled antenna with the same spatial setting. Specifically, the number of scans per foot was 72, whereas the time range was 12 ns, which was digitized into 512 samples. Noting this information is important for the application phase. If a new GPR data set is collected using different settings, the new GPR images will need to be resampled to have the same size of the training ones. The extraction of those 4000 examples was done automatically, using the rebar picking method described in the previous section. Since the process resulted in the extraction of both positive and negative examples, the classification was then performed by visually examining individual images. Some of positive and negative examples are shown in Fig. 6.

Fourteen layers in total were employed in the design of the CNN, after conducting experiments and comparing the results, as depicted in Fig. 7. As can be seen, in addition to the input and output layers at the two ends, a block of three layers: convolution, rectified linear units, and max pooling layers, is repeated three times in the CNN. The last block of these three layers is then connected to a fully connected layer of 10 neurons, which is further followed by another fully connected layer of two neurons. Finally, a softmax layer is included to facilitate the training of CNN [22].

Following 40 epochs of training with an initial learning rate of 0.0001 and a mini-batch size of 500, the obtained CNN showed a great ability to classify new data. Specifically, the CNN was able to predict the category of 1000 images in the test set with an accuracy of 99.6%. After a visual examination, it was found that in all instances the wrong data classification in the test set had been associated with a false negative rebar detection. In those cases, the CNN failed to recognize the hyperbolic rebar signatures due to a very high degree of signal attenuation for those particular rebars.

3. Case study implementation

The proposed methodology was implemented to automatically pick rebars in the GPR data from surveys of twenty-six concrete bridge decks. The data have been collected by a team from Rutgers University

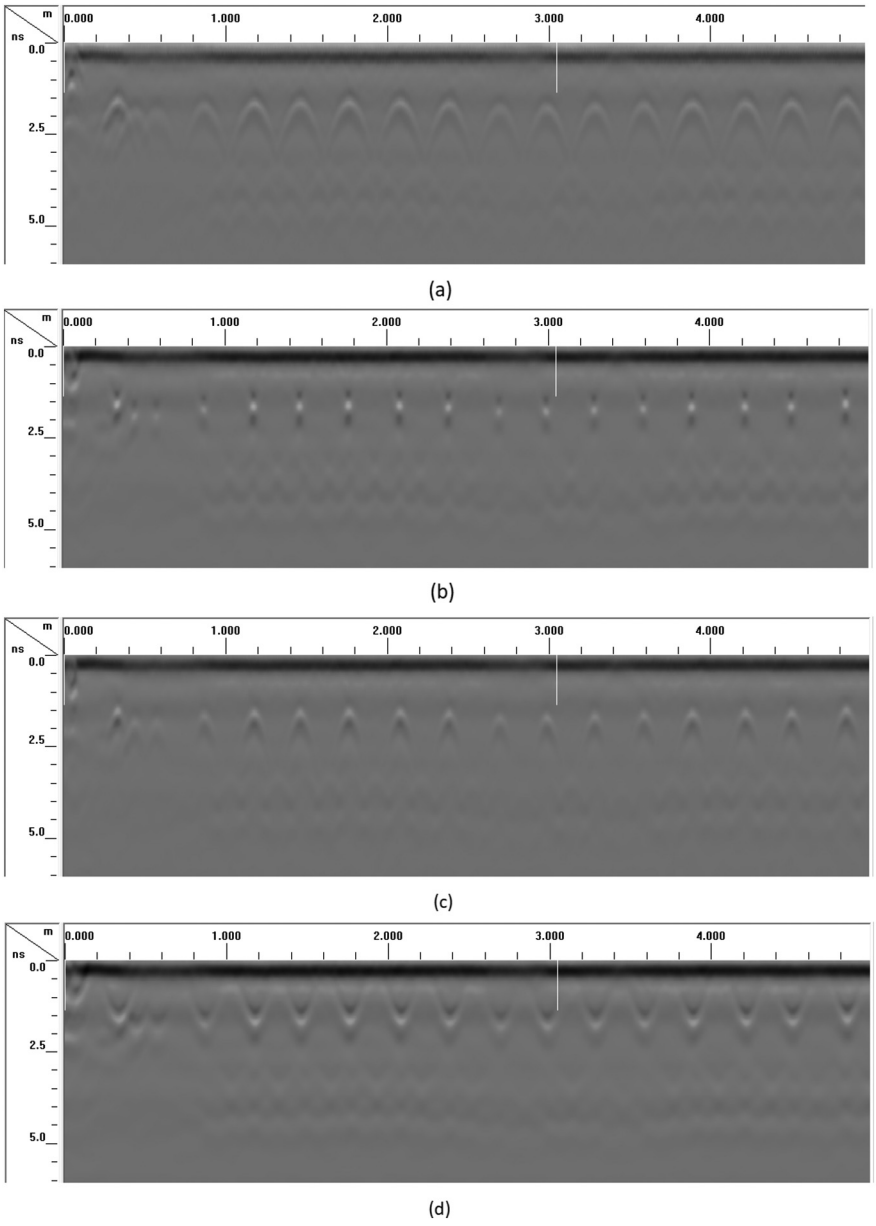

Fig. 3. B-scans: (a) original and (b) after migration.

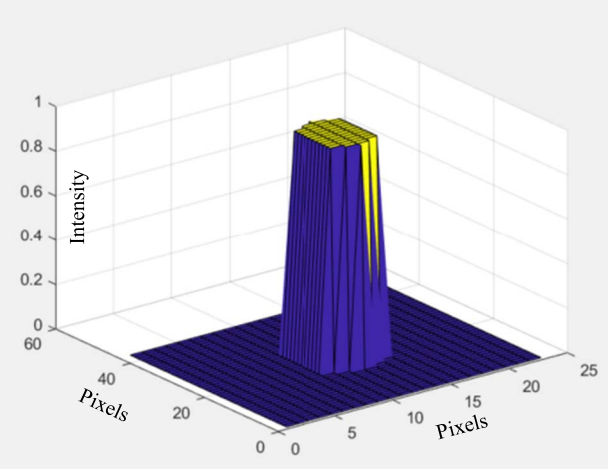

Fig. 4. A match filter to extract rebar objects.

as a part of surveys for the Federal Highway Administration's (FHWA's) Long-Term Bridge Performance (LTBP) Program, and the New Jersey Department of Transportation's (NJDOT's) Bridge Resource Program (BRP). All the data were collected using a GSSI 1.5-GHz ground-coupled antenna with a one-point (constant) gain setting. Although different gain values were used in the data collection on different bridge decks, those did not in any way affect the performance of the proposed picking algorithm. In other words, no further processing was required beyond the processing steps described herein.

The results of the automatic rebar picking for each deck are summarized in Table 1. To simplify the presentation, the names of the bridges are not shown in the table. As can be seen, the results are compared with the ground-truth information to establish the accuracy of the proposed methodology. For a comprehensive evaluation, two measures of accuracy are utilized, as defined by Eqs. (1) and (2). The first measure considers only false negative detections, whereas the second takes into account both false positive and false negative cases. It is noted that the ground-truth information is defined by the visual examination of each individual B-scan. This procedure is appropriate

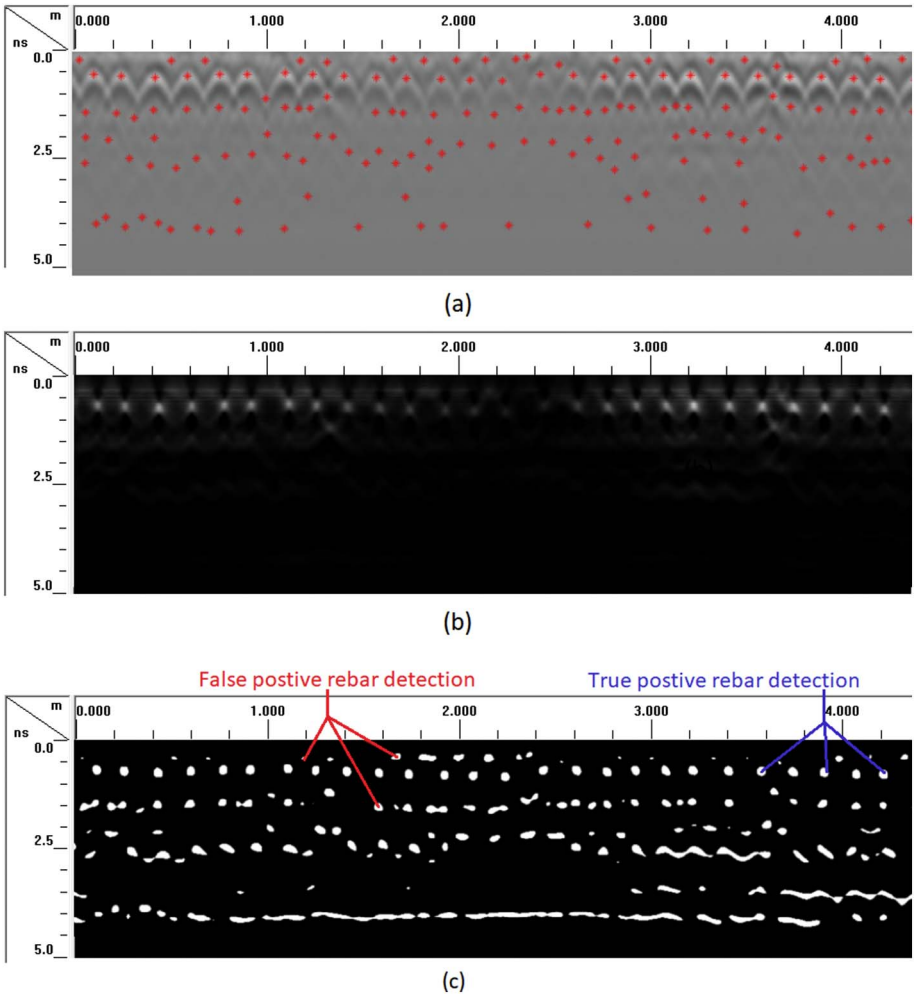

Fig. 5. GPR images (a) original, (b) after migration, and (c) binary objects after filtering and thresholding.

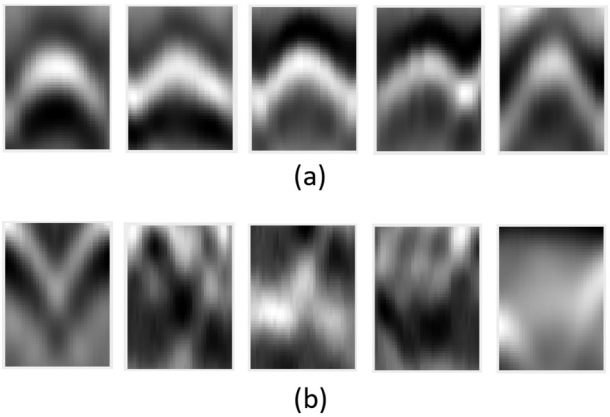

Fig. 6. GPR images for training of the CNN: (a) positive examples, (b) negative examples.

because the goal of the study was to develop an algorithm that would ultimately replace the manual execution of the task. As can be seen in Table 1, the results show that the overall accuracy of rebar picking method is 99.67% and 99.60%, for the first and second measure of accuracy, respectively. The smallest accuracy was observed to be 95.75% for the 26th bridge deck in the library. These accuracies are significantly greater than those reported in [18], which applied the latest automatic rebar picking technique. In addition, the standard deviation for both accuracies was 0.85%.

$$Accuracy_{Type\ I} = \frac{Number\ of\ true\ positive\ peaks}{Total\ number\ of\ ground-truth\ rebar\ peaks} \quad (1)$$

$$Accuracy_{Type\ II} = \frac{Number\ of\ true\ postive\ peaks - Number\ of\ false\ positive\ peaks}{Total\ number\ of\ ground-truth\ rebar\ peaks} \quad (2)$$

4. Conclusions

Picking rebars manually from the GPR data is time consuming and labor intensive. Therefore, a novel method to automate that task was developed and presented. Based on the deep learning techniques, a CNN was trained to recognize rebar signatures in GPR B-scans of concrete bridge decks. To pick rebars in the GPR data for a deck, the trained CNN is employed after conventional image processing techniques have been used to locate potential rebar peaks. Its function is to retain the likely true positive, and to discard likely false positive rebar detections from the previous step. The implementation of the developed algorithm on the GPR data from surveys of twenty-six bridge decks indicated excellent performance, with an overall accuracy of detection of 99.60% ± 0.85%. The main limitation of the proposed algorithm is that it requires a large amount of data for the training of CNN, and that those data need to be representative for bridge decks that will be surveyed in the future. For example, the CNN obtained in this study would likely fail to detect rebar signatures in concrete decks with an asphalt overlay. Such a limitation will be addressed in future studies.

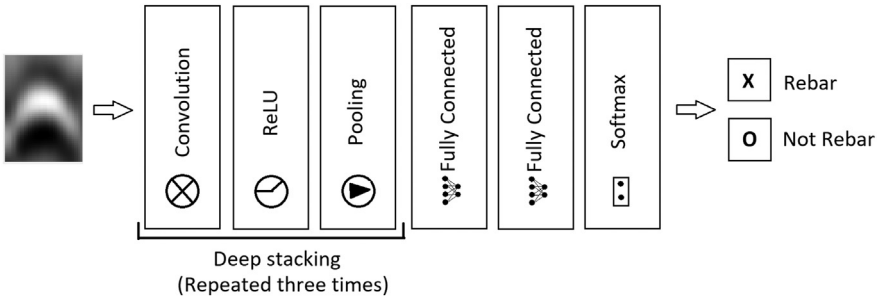

Fig. 7. Structure and operation of the CNN.

Table 1
Performance of the proposed algorithm for twenty-six bridge decks.

Bridge #	Ground-truth number of rebar peaks	True positive	False positive	False negative	Accuracy type I	Accuracy type II
1	4002	4002	0	0	100.00%	100.00%
2	6526	6524	0	2	99.97%	99.97%
3	7740	7716	13	24	99.69%	99.52%
4	4603	4594	5	9	99.80%	99.70%
5	5820	5807	12	13	99.78%	99.57%
6	7565	7560	0	5	99.93%	99.93%
7	12,004	11,980	10	24	99.80%	99.72%
8	11,988	11,983	4	5	99.96%	99.92%
9	2772	2736	1	36	98.70%	98.67%
10	6592	6591	0	1	99.98%	99.98%
11	10,343	10,340	3	3	99.97%	99.94%
12	2599	2593	0	6	99.77%	99.77%
13	6867	6788	2	79	98.85%	98.82%
14	5735	5687	4	48	99.16%	99.09%
15	4484	4480	6	4	99.91%	99.78%
16	3422	3414	4	8	99.77%	99.65%
17	3392	3372	0	20	99.41%	99.41%
18	8056	8051	7	5	99.94%	99.85%
19	3418	3412	12	6	99.82%	99.47%
20	3266	3266	4	0	100.00%	99.88%
21	9412	9408	8	4	99.96%	99.87%
22	6720	6720	0	0	100.00%	100.00%
23	4096	4096	0	0	100.00%	100.00%
24	2348	2330	0	18	99.23%	99.23%
25	1376	1372	8	4	99.71%	99.13%
26	4074	3903	2	171	95.80%	95.75%
Overall	149,105	148,610	105	495	99.67%	99.60%
Standard deviation					0.85%	0.85%

Acknowledgements

The authors are grateful to the Federal Highway Administration and New Jersey Department of Transportation for their support in the conduct of GPR surveys through the LTBP and BRP programs, respectively.

References

[1] N. Gucunski, A. Imani, F. Romero, S. Nazarian, D. Yuan, H. Wiggenhauser, P. Shokouhi, A. Taffe, D. Kutrubes, Nondestructive Testing to Identify Concrete Bridge Deck Deterioration, Transportation Research Board, Washington D.C., 2013, http://dx.doi.org/10.17226/22771.

[2] N. Gucunski, B. Pailes, J. Kim, H. Azari, K. Dinh, Capture and quantification of deterioration progression in concrete bridge decks through periodical NDE surveys, J. Infrastruct. Syst. 23 (1) (2016 Jun 17) B4016005, , http://dx.doi.org/10.1061/(ASCE)IS.1943-555X.0000321.

[3] C.L. Barnes, J.F. Trottier, Effectiveness of ground penetrating radar in predicting deck repair quantities, J. Infrastruct. Syst. 10 (2) (2004 Jun) 69–76, http://dx.doi.org/10.1061/(ASCE)1076-0342(2004)10:2(69).

[4] C.L. Barnes, J.F. Trottier, D. Forgeron, Improved concrete bridge deck evaluation using GPR by accounting for signal depth–amplitude effects, NDT&E Int. 41 (6) (2008 Sep 30) 427–433, http://dx.doi.org/10.1016/j.ndteint.2008.03.005.

[5] A. Tarussov, M. Vandry, A. De La Haza, Condition assessment of concrete structures using a new analysis method: ground-penetrating radar computer-assisted visual interpretation, Constr. Build. Mater. 38 (2013) 1246–1254, http://dx.doi.org/10.1016/j.conbuildmat.2012.05.026.

[6] N. Martino, K. Maser, R. Birken, M. Wang, Quantifying bridge deck corrosion using ground penetrating radar, Res. Nondestruct. Eval. 27 (2) (2016 Apr 2) 112–124, http://dx.doi.org/10.1080/09349847.2015.1067342.

[7] K. Dinh, T. Zayed, S. Moufti, A. Shami, A. Jabri, M. Abouhamad, T. Dawood, Clustering-based threshold model for condition assessment of concrete bridge decks with ground-penetrating radar, Transp. Res. Rec. (2522) (2015 Aug 1) 81–89, http://dx.doi.org/10.3141/2522-08.

[8] K. Dinh, N. Gucunski, J. Kim, T.H. Duong, Understanding depth-amplitude effects in assessment of GPR data from concrete bridge decks, NDT&E Int. 83 (2016 Oct 31) 48–58, http://dx.doi.org/10.1016/j.ndteint.2016.06.004.

[9] K. Dinh, T. Zayed, F. Romero, A. Tarussov, Method for analyzing time-series GPR data of concrete bridge decks, J. Bridg. Eng. 20 (6) (2014) 04014086, , http://dx.doi.org/10.1061/(ASCE)BE.1943-5592.0000679.

[10] K. Dinh, N. Gucunski, J. Kim, T.H. Duong, Method for attenuation assessment of GPR data from concrete bridge decks, NDT&E Int. 92 (2017 Dec 1) 50–58, http://dx.doi.org/10.1016/j.ndteint.2017.07.016.

[11] N. Gucunski, B. Basily, J. Kim, G.Y. Jin, T. Duong, K. Dinh, S.H. Kee, A. Maher, RABIT: implementation, performance validation and integration with other robotic platforms for improved management of bridge decks, Int. J. Intell. Robot. Appl. 1 (3) (2017 Jul 17) 271–286, http://dx.doi.org/10.1007/s41315-017-0027-5.

[12] W. Al-Nuaimy, Y. Huang, M. Nakhkash, M.T.C. Fang, V.T. Nguyen, A. Eriksen, Automatic detection of buried utilities and solid objects with GPR using neural networks and pattern recognition, J. Appl. Geophys. 43 (2) (2000) 157–165, http://dx.doi.org/10.1016/S0926-9851(99)00055-5.

[13] P. Gamba, S. Lossani, Neural detection of pipe signatures in ground penetrating radar images, IEEE Trans. Geosci. Remote Sens. 38 (2) (2000) 790–797, http://dx.doi.org/10.1109/36.842008.

[14] E. Pasolli, F. Melgani, M. Donelli, Automatic analysis of GPR images: a pattern-recognition approach, IEEE Trans. Geosci. Remote Sens. 47 (7) (2009) 2206–2217, http://dx.doi.org/10.1109/TGRS.2009.2012701.

[15] V. Krause, I. Abdel-Qader, O. Abudayyeh, S. Yehia, An image segmentation algorithm for the detection of rebar in bridge decks from GPR scans, Electro/Information Technology, IEEE International Conference, 2007, pp. 114–119, , http://dx.doi.org/10.1109/EIT.2007.4374476 (IEEE).

[16] M.R. Shaw, S.G. Millard, T.C.K. Molyneaux, M.J. Taylor, J.H. Bungey, Location of steel reinforcement in concrete using ground penetrating radar and neural networks, NDT&E Int. 38 (3) (2005) 203–212, http://dx.doi.org/10.1016/j.ndteint.2004.06.011.

[17] Z.W. Wang, M. Zhou, G.G. Slabaugh, J. Zhai, T. Fang, Automatic detection of bridge deck condition from ground penetrating radar images, IEEE Trans. Autom. Sci. Eng. 8 (3) (2011) 633–640, http://dx.doi.org/10.1109/TASE.2010.2092428.

[18] P. Kaur, K.J. Dana, F.A. Romero, N. Gucunski, Automated GPR rebar analysis for robotic bridge deck evaluation, IEEE Trans. Cybern. 46 (10) (2016) 2265–2276, http://dx.doi.org/10.1109/TCYB.2015.2474747.

[19] R. Yelf, Where is true time zero? Ground Penetrating Radar, 2004. GPR 2004. Proceedings of the Tenth International Conference on (Vol. 1, pp. 279–282), IEEE, 2004.

[20] C. Özdemir, Ş. Demirci, E. Yiğit, B. Yilmaz, A review on migration methods in B-scan ground penetrating radar imaging, Math. Probl. Eng. (2014), http://dx.doi.org/10.1155/2014/280738.

[21] Y. LeCun, Y. Bengio, G. Hinton, Deep learning, Nature 521 (7553) (2015) 436–444, http://dx.doi.org/10.1038/nature14539.

[22] C.M. Bishop, Pattern Recognition and Machine Learning, Springer, 978-0-387-31073-2, 2006.